Effect of lateral boundaries on contrast functions in time-resolved transillumination measurements

Victor Chernomordik and Amir H. Gandjbakhche
National Institute of Child Health and Human Development, Laboratory of Integrative and Medical Biophysics, National Institutes of Health, Bethesda, Maryland 20892

Jeremy C. Hebden
Department of Medical Physics, University College London, 11-20 Capper Street, London WC1E 6JA, United Kingdom

Giovanni Zaccanti
Dipartimento di Fisica dell'Università degli Studi di Firenze and INFM, Via Santa Marta 3, 50139 Firenze, Italy

(Received 28 August 1998; accepted for publication 18 June 1999)

The method of images is employed to insert the effects of the presence of a single lateral boundary on contrast functions previously derived for an infinite slab using a random walk model of photon transport. The predictions of the model for zero and extrapolated boundary conditions are compared with Monte Carlo (MC) simulations and with experimental results obtained using a homogenous phantom with tissue-like optical properties. As expected, the extrapolated boundary condition yields better agreement between the theoretical predictions and results obtained from MC and experiments. This indicates that the random walk model has potential as a forward model in iterative imaging schemes developed for optical tomography. © *1999 American Association of Physicists in Medicine.* [S0094-2405(99)01709-5]

Key words: time-resolved transillumination, quantitative imaging, random walk, Monte Carlo simulations, contrast functions

I. INTRODUCTION

Near-infrared (NIR) spectroscopy has demonstrated valuable contributions to medical diagnosis over the past couple of decades.[1–3] The different absorption characteristics of oxy- and deoxy-haemoglobin enable measurements of transmitted light at certain NIR wavelengths to yield important clinical information related to tissue function. Naturally, researchers working in this field have become increasingly interested in localizing the region of tissue under examination, and the development of a generalized optical imaging technique is currently receiving considerable attention in the biomedical optics community.[2–6] However, optical tomography is a very difficult problem. Unlike the forms of ionizing radiation employed by current medical imaging methods such as CT, SPECT, and PET optical radiation is scattered profusely in tissue. A collimated beam of light can only propagate a millimeter or so through most tissues before the initial directionality of the beam is completely lost. The predominance of scatter ensures that absolute measurements of transmitted intensity across several centimeters of tissue are much more strongly influenced by photon interactions at the surface than by the specific optical properties of localized regions deeper within the tissue. As a result, continuous wave (cw) imaging systems developed commercially in the past demonstrated very poor spatial resolution and contrast,[7] which motivated researchers to investigate measurements with a greater information content. Specifically, researchers have explored the potential of time and frequency domain measurements.[4,5,8]

The assumption that underlies optical tomography is that a finite set of measurements of transmitted light between pairs of points on the surface of an object is sufficient to reconstruct an arbitrary three-dimensional (3D) distribution of internal scatterers and absorbers. Unfortunately, the use of the Radon transform and backprojection methods is invalid for all but a limited and largely trivial set of circumstances. Therefore, some investigators have sought a general solution of the inverse problem by attempting to recover the parameters describing an appropriate model of photon transport by comparing its predictions with the measured data. The model may then be adjusted subsequently in an iterative fashion until acceptable correspondence is achieved. This approach requires two distinct components: (i) a forward model which can generate a set of reliable measurements from a given internal 2D or 3D distribution of scattering and absorbing parameters, and (ii) a scheme for adjusting the parameters of the forward model based on a minimization of the error between the model predictions and the experimental data. The latter component can be approached in a number of ways, as recently reviewed by Arridge and Hebden.[6] Although methods may vary in terms of speed of computation, reconstruction is more critically dependent on the accuracy of the forward model than on the error minimization scheme. A variety of theories and models for light transport in tissue have been explored.[6] By far the most flexible in terms of modeling arbitrarily complex objects are Monte Carlo methods.[9–11] However, the substantial computation required in order to obtain adequate statistics prohibits their use in iterative reconstruction schemes. Computation time can be

reduced significantly by employing deterministic models, of which the most general is the numerical solution of the radiative transfer equation.[12,13] Further reduction of the computation time can be achieved by the diffusion approximation to the radiative transfer equation.[14] Another alternative is a random-walk model, in which the tissue is represented by a simple cubic lattice and photons move randomly between adjacent lattice points. A relatively straightforward mathematical analysis of random walk[15,16] yields a powerful description of photon migration. When photon motion occurs with each of the lattice directions having equal probability, random walk can, in some sense, be considered to be equivalent to a finite difference approximation of the diffusion equation but gives the possibility to obtain simple analytical formulas describing photon propagation in many practically important cases (see, e.g., review of Ref. 16).

Recent achievements of the random walk theory (RWT) developed at the National Institutes of Health (NIH) include demonstrations of its ability to accurately model the time-resolved transmittance across uniform slabs of tissue, as well as slabs containing isolated targets of different scattering or absorbing properties.[17–19] Many predictions of RWT have been confirmed using time-resolved measurements on suitable slab phantoms with tissue-like optical properties. Recently, a methodology was developed which facilitates an accurate quantification of the optical properties and the cross section of abnormally scattering and/or absorbing targets.[20] This methodology is based on the derivation of time-dependent contrast functions. However, the model have assumed media consisting of infinite slabs, and it has been necessary to compare its predictions with data recorded along lines of sight sufficiently far from lateral boundaries of phantoms. It has generally been assumed that sufficient in this case implies a distance from the boundary of at least half the thickness of the slab. If RWT is to be developed into an effective forward model for optical tomography it is essential that it be adaptable to realistic finite tissue geometries. In a significant step towards this goal we present an attempt to model the effects of a plane lateral boundary on the contrast functions obtained from time-resolved measurements of transmitted intensity. Effects of a single lateral boundary are inserted to the two pertinent quantities needed for the computation of the contrast functions. Namely, the time of flight expression for an homogeneous slab, and the expression of the point spread function (PSF). The predictions of the model are compared with those of Monte Carlo simulations and with the results of an experiment performed on a tissue-like slab.

II. RANDOM WALK MODEL

A. Time-of-flight probability for a slab with a side boundary

The application of RWT to a homogenous slab of tissue without lateral boundaries is described in detail by Gandjbakhche *et al.*[17] Photon position and flight time are described in terms of dimensionless coordinates (x,y,z) and the number of steps n respectively. The slab is considered to be N lattice units thick, bounded by planes at $z=0$ and $z=N$, and the absence of lateral boundaries implies that coordinates x and y can assume all integer values from $-\infty$ to ∞. Each photon enters the medium at a point $\mathbf{r}_0$ and exits at point $\mathbf{r}=(x,y,N)$ after n steps.

Let $p_n(\mathbf{r},\mathbf{r}_0)$ be the probability that a photon injected at $\mathbf{r}_0$ at $n=0$ is at $\mathbf{r}$ after step n. In the earlier analysis for an infinite slab,[17] the joint probability was derived that a photon transmitted through the slab emerges at a horizontal shift ρ (expressed in lattice units) from the point of insertion. Assuming the source is located at point $\mathbf{r}_0=(0,0,0)$, the probability of detecting a photon at the exit point $\mathbf{r}=(\rho,0,N)$ is given by

$$
\begin{aligned}
p_n(\mathbf{r},\mathbf{0}) &= p_n(\rho,0,N,\mathbf{0}) \\
&= \frac{\sqrt{3}}{2}(2\pi n)^{-3/2}\exp\left[-\mu n-\frac{3\rho^2}{2n}\right] \\
&\quad\times\sum_{k=-\infty}^{\infty}\left\{\exp\left[-\frac{3[(2k+1)N-2]^2}{2n}\right]\right. \\
&\quad\left.-\exp\left[-\frac{3[(2k+1)N]^2}{2n}\right]\right\},
\end{aligned}
\tag{1}
$$

where μ describes the loss of photons (per lattice unit) due to absorption.

We now seek to redefine $p_n(\mathbf{r},\mathbf{0})$ as $p_n(\mathbf{r},\mathbf{0},R)$ for the case of a lateral boundary situated at a distance R lattice units from the source. The geometry of corresponding experimental setup is presented in Fig. 1 (abnormally absorbing and/or scattering target inside the slab, analyzed below in Sec. II B is also shown). For simplicity, we assume that the two lateral boundaries are far enough from each other that photon trajectories are perturbed only by one of these boundaries. Although the resulting expressions would be quite complicated, the mathematical construct for the presence of both lateral boundaries is a straightforward extension of the analysis below. In fact, it is similar to transition from the propagator in the semi-infinite space to the propagator in the infinite rectangular slab that can be presented as an infinite series in terms of the free space propagators.[16] Thus, the result for the slab with two lateral boundaries can be reduced to an infinite series of the infinite slab propagators.

The standard technique to take into account the presence of a boundary is the method of images.[21] In which some imaginary sources are added to the real one in order to provide the fulfillment of the necessary boundary conditions. Three types of these conditions were suggested for the case of absorbing plane boundary in the literature, i.e., ''zero boundary'', ''extrapolated boundary,'' and ''partial current boundary.''[22–27] The first two of them suggest zero fluence at some plane. For the ''zero boundary'' condition, this zero-fluence plane is the boundary plane itself. For the ''extrapolated boundary'' condition, it is the plane parallel to the boundary but shifted outward from the scattering medium. Magnitude of this shift d_e depends on the reflective properties of the boundary and scattering coefficient of the

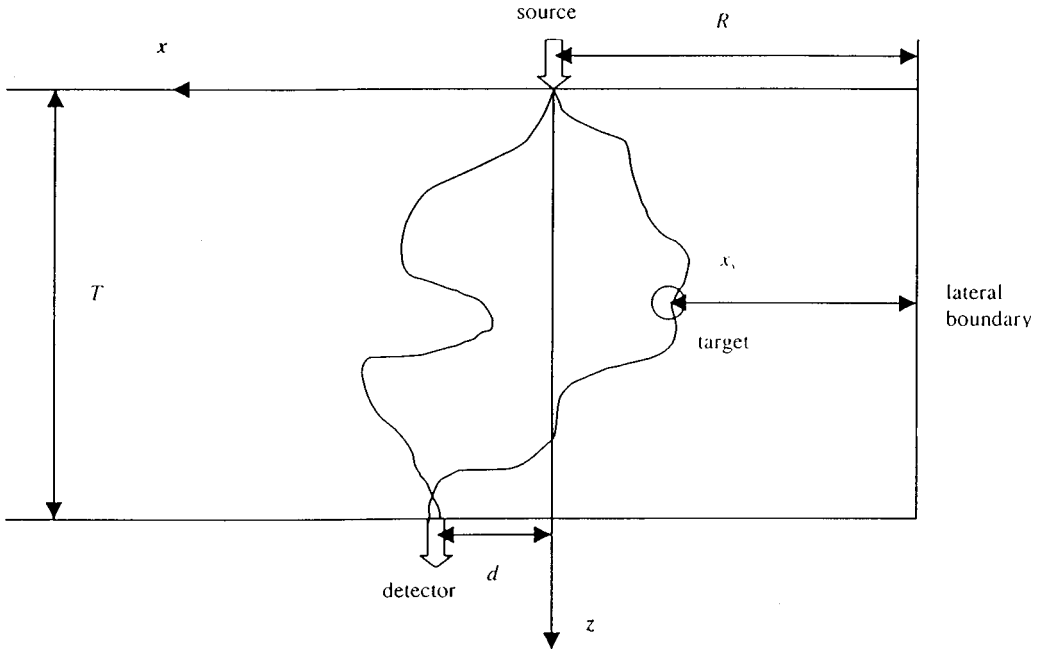

FIG. 1. Geometric scheme assumed for theoretical model, Monte Carlo simulations and corresponding experimental setup.

medium.[22,23] For totally absorbing boundary (no refraction index mismatch), it is shown in the paper[23] that $d_e \cong 0.71/\mu_s'$. In the RWT framework, it is reasonable to estimate d_e as a half of the lattice step (exiting photon leaves the boundary lattice point and disappears, being absorbed halfway to the next (external) lattice point) that gives similar result $d_e = (\sqrt{2}\mu_s')^{-1} \cong 0.71/\mu_s'$. The so-called ''partial current'' boundary condition deals with both the flux and fluence at the physical boundary of the scattering medium. It is shown to give very close results to the ''extrapolated boundary'' condition.[22] These results proved to be more accurate than given by the application of the simple ''zero boundary'' condition.

Thus, the effect of an absorbing plane boundary may be reproduced by placing a negative source beyond the slab. To provide the ''zero boundary'' condition, the position of this source should be symmetrical to the position of the real source relative to the boundary plane. Similarly, to provide the ''extrapolated boundary'' condition, the image and the real sources should be symmetrical relative to the ''extrapolated boundary'' plane. It should be noted that for a perfectly reflecting boundary, the corresponding image source is positive, and it is positioned symmetrically relative to boundary plane to provide zero flux through the boundary.[16]

Applying the method of images to the quantity $p_n(\mathbf{r},\mathbf{0},R)$, the new expression for the detection probability in the presence of lateral boundary can be calculated as follows:

$$p_n(\mathbf{r},\mathbf{0},R) = p_n(\mathbf{r},\mathbf{0}) \mp p_n(\mathbf{r},\mathbf{r}'), \tag{2}$$

where $\mathbf{r}' = (-2R-\rho,0,N)$ for the ''zero boundary'' condition or $\mathbf{r}' = (-2(R+\tilde{d}_e)-\rho,0,N)$ for the ''extrapolated boundary'' condition, $\tilde{d}_e$ is the mentioned above shift of the extrapolated boundary plane relative to the physical boundary in the lattice units. The sign in the r.h.s. of Eq. (2) is ''+'' only for the perfectly reflecting boundary, when the image source is positive.[16]

In accordance with Fig. 1, the sign convention for ρ is the following: ρ is positive if the source is closer to the side boundary than the detector and negative otherwise.

Before taking the analysis any further, we will first convert each of the dimensionless parameters in the model to real physical variables. The propagation of light through tissue can be described in terms of four fundamental characteristics: the refractive index, the absorption coefficient μ_a, the scatter coefficient μ_s, and the scatter anisotropy factor g. However, over distances of a few millimeters or greater, photon transport can be conveniently described in terms of the transport scatter coefficient $\mu_s' = \mu_s(1-g)$. This parameter can be considered as the scatter coefficient for isotropic scattering in the medium. It can be shown that the appropriate transformations are:[17]

$$\mu \to \frac{\mu_a}{\mu_s'}, \quad n \to \mu_s' c\Delta t, \quad \mathbf{r} \to \bar{\mathbf{r}}\frac{\mu_s'}{\sqrt{2}}, \quad \rho \to d\frac{\mu_s'}{\sqrt{2}},$$
$$N \to T\frac{\mu_s'}{\sqrt{2}} + 1, \quad R \to \bar{R}\frac{\mu_s'}{\sqrt{2}}, \tag{3}$$

where c is the speed of light in the medium (mm/ps), Δt is the excess photon transit time (ps), $\bar{\mathbf{r}}$ is the distance variable (mm), R is the distance between the source and the side boundary (mm), d is the horizontal displacement between the source and the detector (mm), and T is the thickness of the slab (mm). By replacing all these quantities in Eqs. (1) and (2), it can be shown that the time-of-flight probability

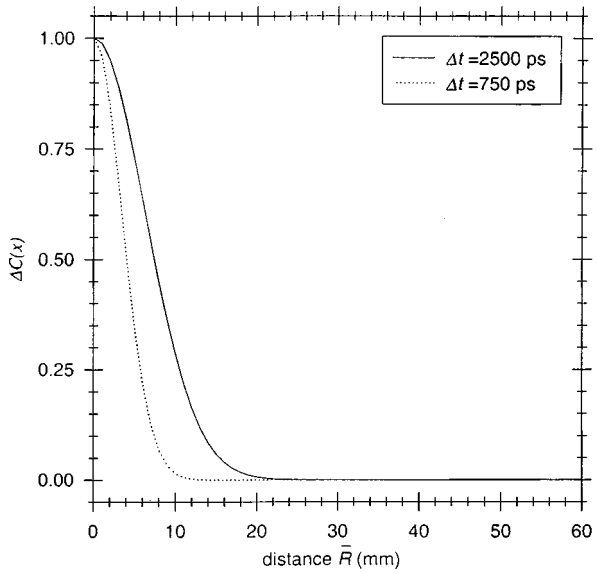

FIG. 2. Contrast correction due to the side boundary (additive component).

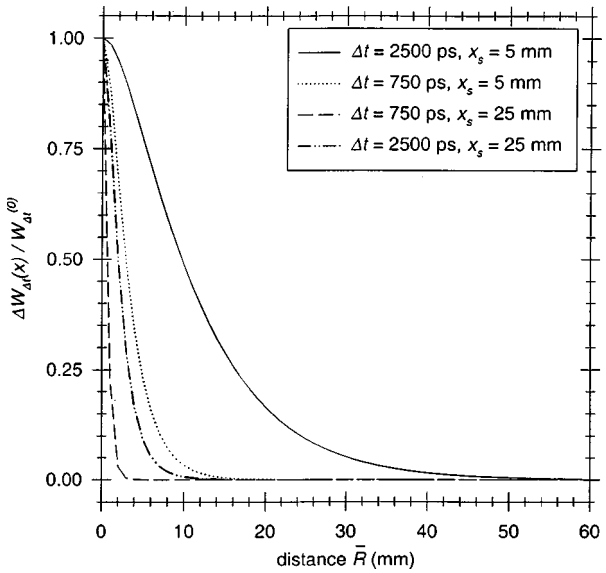

FIG. 3. Dependence of the ratio $\Delta W_{\Delta t}/W_{\Delta t}$ on the distance from the side boundary resulted in the multiplicative component of the contrast correction.

$\tilde{p}_{\Delta t}(d,T,\bar{R})$ with the presence of a side boundary under an assumption of the ''zero boundary'' condition is given by

$$\tilde{p}_{\Delta t}(d,T,\bar{R}) = p_{\Delta t}(d,T)\exp\left(-\frac{3\mu_s' d^2}{4c\Delta t}\right) \times\left\{1-\exp\left[-\frac{3\mu_s'[(2\bar{R}+d)^2-d^2]}{4c\Delta t}\right]\right\}, \quad (4)$$

where $p_{\Delta t}(d,T)=p_{\Delta t}(\hat{\mathbf{r}},\mathbf{0})$, $\hat{\mathbf{r}}=(d,0,T)$.

In the specific case that the source and detector are aligned on axis ($d=0$), Eq. (4) becomes

$$\tilde{p}_{\Delta t}(0,T,\bar{R}) = p_{\Delta t}(0,T)\left[1-\exp\left(-\frac{3\mu_s'\bar{R}^2}{c\Delta t}\right)\right]. \quad (5)$$

As expected, the probability approaches that for an infinite slab for very large values of R, and falls to zero as the source approaches the side boundary ($\bar{R}\to 0$). From Eq. (5) it is a straightforward matter to calculate the total transmitted intensity $I(\bar{R})$ and the mean flight time $\langle\Delta t\rangle(\bar{R})$, as a function of the boundary distance $\bar{R}$ as follows:

$$I_{CW}(\bar{R}) = \int_0^\infty d(\Delta t)\tilde{p}_{\Delta t}(T,\bar{R}), \quad (6)$$

$$\langle\Delta t\rangle(\bar{R}) = \frac{\int_0^\infty d(\Delta t)\Delta t\tilde{p}_{\Delta t}(T,\bar{R})}{\int_0^\infty d(\Delta t)\tilde{p}_{\Delta t}(T,\bar{R})}. \quad (7)$$

It is evident that, for the ''extrapolated boundary'' condition, $\bar{R}$ in r.h.s. of Eqs. (4)–(7) should be replaced by $\bar{R}+d_e$. Presented above expressions for $I_{\rm cw}(\bar{R})$ and $\langle\Delta t\rangle(\bar{R})$ are compared with numerical and experimental results in Sec. III.

B. Time-dependent contrast functions

Previous studies described in detail elsewhere[19,20] have employed RWT to determine the ability of optical time-of-flight measurements to detect anomalously absorbing or diffusing targets embedded in an otherwise uniform medium. A quantity known as the time dependent contrast was defined as the normalized difference between transmitted fluxes in the absence and presence of the target. The contrast functions for absorbing and diffusing targets are approximated respectively by:

$$C_A(\mathbf{r},\mathbf{r}_0,n) \approx \eta\frac{W(\mathbf{s},\mathbf{r},\mathbf{r}_0)_{n+1}}{p_n(\mathbf{r},\mathbf{r}_0)}, \quad (8)$$

$$C_D(\mathbf{r},\mathbf{r}_0,n) \approx \langle\Delta n_D\rangle\frac{W(\mathbf{s},\mathbf{r},\mathbf{r}_0)_n - W(\mathbf{s},\mathbf{r},\mathbf{r}_0)_{n-1}}{p_n(\mathbf{r},\mathbf{r}_0)}, \quad (9)$$

where $W(\mathbf{s},\mathbf{r},\mathbf{r}_0)_n$ is the probability that a photon, after entering the slab at $\mathbf{r}_0$ visits the site of the target at $\mathbf{s}=(s_1,s_2,s_3)$ and is detected at $\mathbf{r}$ at step n. The constants η and $\langle\Delta n_D\rangle$ are quantities related to the optical properties and the size of the target.[20] The functions C_A and C_D are known as the absorptive and diffusion contrast functions, respectively.

To obtain expressions for the contrast functions in the presence of a side boundary, the quantity $W(\mathbf{s},\mathbf{r},\mathbf{r}_0)_n$ needs to be modified. From the previous analysis,[20] $W(\mathbf{s},\mathbf{r},\mathbf{r}_0)_n$ is given by

$$W(\mathbf{s},\mathbf{r},\mathbf{r}_0)_n = \sum_{l=0}^{n} p_l(\mathbf{r},\mathbf{s})p_{n-l}(\mathbf{s},\mathbf{r}_0) = \frac{9}{16\pi^{3/2}n^{3/2}}\sum_{k=-\infty}^{\infty}\sum_{m=-\infty}^{\infty}\{F_n[\alpha_-(k),\beta_-(m,\rho)] + F_n[\alpha_+(k),\beta_+(m,\rho)] - F_n[\alpha_+(k),\beta_-(m,\rho)] - F_n[\alpha_-(k),\beta_+(m,\rho)]\}, \quad (10)$$

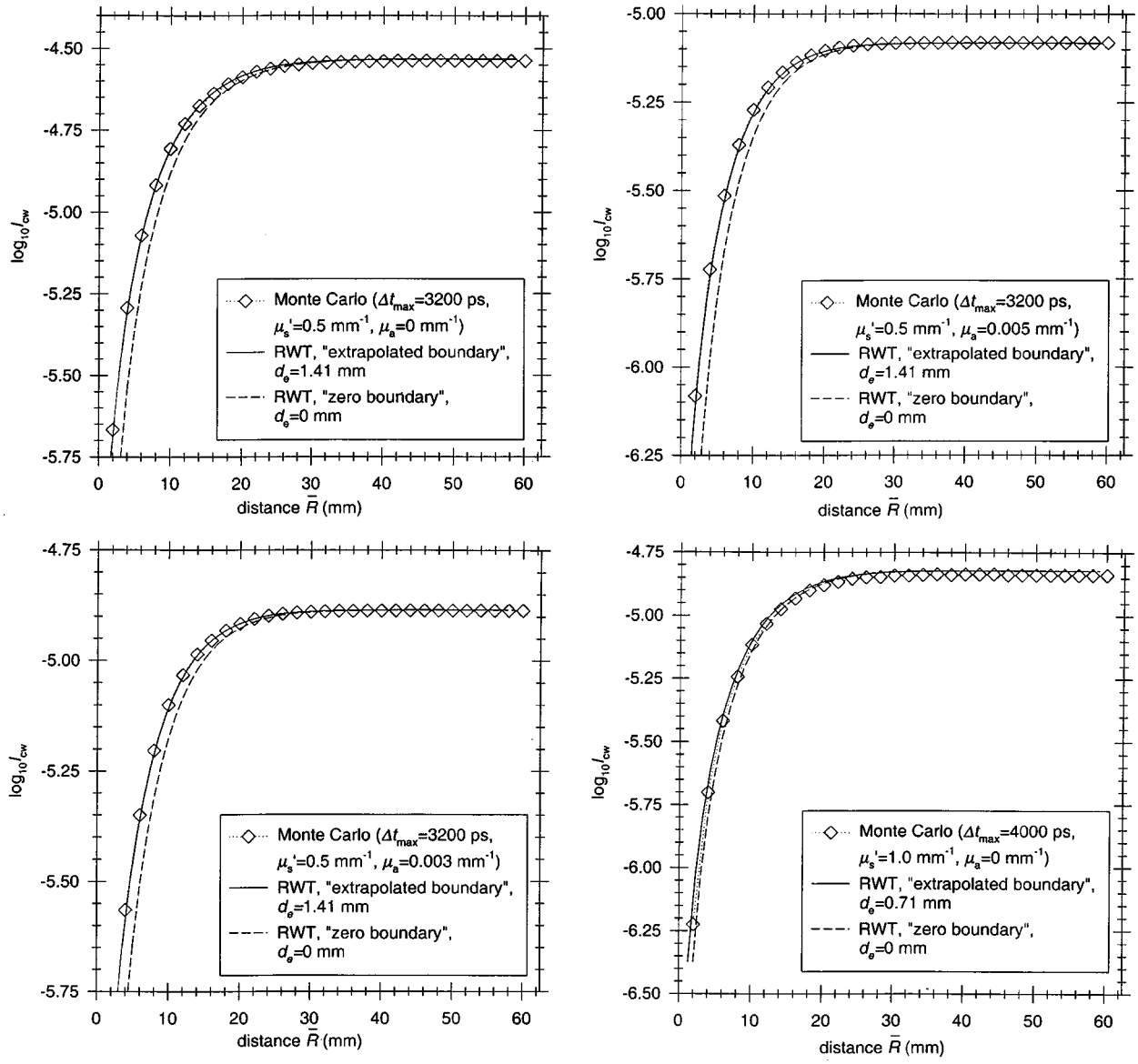

FIG. 4. (a)–(f) Curves of the cw intensity near the side boundary for $\mu_s'=0.5$, and 1.0 mm^{-1}, $\mu_a=0.0$, 0.003, and 0.005 mm^{-1}, respectively-comparison of the RWM estimates with the results of the Monte Carlo simulations.

where

$$F_n(a,b)=\left(\frac{1}{a}+\frac{1}{b}\right)\exp\left[-\frac{(a+b)^2}{n}\right],$$

$$\alpha_{\pm}(k)=\{\tfrac{3}{2}[s_1^2+(s_3+2kN\pm 1)^2]\}^{1/2},$$

$$\beta_{\pm}(k)=\{\tfrac{3}{2}[(\rho-s_1)^2+(N-s_3+2kN\pm 1)^2]\}^{1/2}.$$

For simplicity, we have assumed that the target is located in the same plane ($y=0$) as the horizontal displacement between the source and detector, such that $\mathbf{s}=(s_1,0,s_3)$. Again one can replace the dimensionless parameters in Eq. (10) with the physical variables as defined in Eq. (3).

By employing the method of images once again [similar to Eq. (2)] to modify probabilities $p_l(\mathbf{r},\mathbf{s})$ and $p_{n-l}(\mathbf{s},\mathbf{r}_0)$ in the Eq. (10) for the case of the absorbing lateral boundary, we obtain an expression for $\tilde{W}_{\Delta t}(x_1,0,x_3,d,T,\overline{R})$ which represents the algebraic sum of four functions corresponding to the four combinations of the real source, the detector and their images:

$$\begin{aligned}\tilde{W}_{\Delta t}(x_1,0,x_3,d,T,\overline{R})&=W_{\Delta t}(x_1,0,x_3,d,T)+W_{\Delta t}(2\overline{R'}+x_1,0,x_3,d+2\overline{R'},T)\\&\quad-W_{\Delta t}(x_1,0,x_3,d+2\overline{R'},T)-W_{\Delta t}(2\overline{R'}+x_1,0,x_3,d,T),\end{aligned}\tag{11}$$

where $\overline{R'}=\overline{R}$ for the ''zero boundary'' condition, $\overline{R'}=\overline{R}+d_e$ for the ''extrapolated boundary'' condition, and the parameters x_1, $x_2=0$, and x_3 are the actual coordinates of the target expressed in millimeters.

It will be shown in Sec. III that the ''extrapolated boundary'' condition gives the more accurate description of the

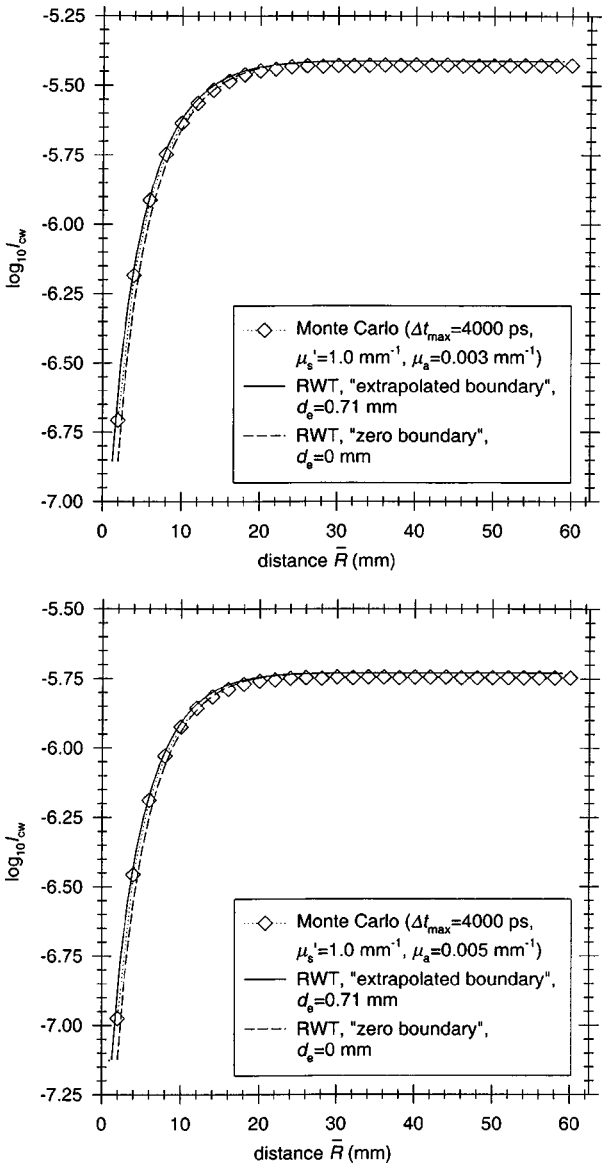

FIG. 4. (*Continued.*)

effect of the lateral boundary than the ''zero boundary'' condition (as was previously shown to be the case for the infinite slabs[22–25]).

Equation (11) can be expressed as the function obtained for an infinite slab plus an extra corrective term:

$$\tilde{W}_{\Delta t}(x_1,0,x_3,d,T,\bar{R}) = W_{\Delta t}(x_1,0,x_3,d,T) + \Delta W_{\Delta t}(x_1,0,x_3,d,T,\bar{R}), \quad (12)$$

where $W_{\Delta t}(x_1,0,x_3,d,T) = W_{\Delta t}(\mathbf{x},\hat{\mathbf{r}},\mathbf{0})$, $\hat{\mathbf{x}} = (x_1,0,x_3)$, $\hat{\mathbf{r}} = (d,0,T)$.

Note that previously it was shown that the complicated expressions for $W(\mathbf{s},\mathbf{r},\mathbf{r}_0)_n$ or in physical coordinates $W_{\Delta t}(\mathbf{x},\hat{\mathbf{r}},\mathbf{0})$ can be approximated by a simple Gaussian function, which considerably simplifies the calculations of contrast and thus significantly reduces the computation involved in solution of the inverse problem.[18]

In the case of a rectangular slab with a lateral boundary, new expressions for the time-dependent contrast functions are derived by inserting expressions for $\tilde{p}_{\Delta t}(d,T,\bar{R})$ and $\tilde{W}_{\Delta t}(x_1,0,x_3,d,T,\bar{R})$ into Eqs. (8) and (9). For a target that is weakly absorbing, we obtain

$$\tilde{C}_A(x_1,0,x_3,d,T,\bar{R})_{\Delta t} = C_A(x_1,0,x_3,d,T)_{\Delta t} \times \left\{1 + \frac{\Delta W_{\Delta t}(x_1,0,x_3,d,T,\bar{R})}{W_{\Delta t}(x_1,0,x_3,d,T)}\right\} + \frac{p_{\Delta t}(d,T) - \tilde{p}_{\Delta t}(d,T,\bar{R})}{p_{\Delta t}(d,T)}. \quad (13)$$

Note that the last term in the r.h.s. of the Eq. (13) (additive correction term), which is also the most significant, does not depend on the position of the target but only on the positions of the source and detector relative to the side boundary. The behavior of this term is illustrated by Fig. 2 for the case of a slab of thickness $T=40\,\text{mm}$, and optical properties $\mu_s' = 1.0\,\text{mm}^{-1}$ and refractive index of 1.0. Note that neither of the correction terms have dependence upon μ_a. The horizontal axis is the distance R between the boundary and the source-detector axis. Two values of time delay Δt have been selected, equal to 750 and 2500 ps. The dependence of the ratio $\Delta W_{\Delta t}/W_{\Delta t}$ [in parenthesis in Eq. (13)] on the distance from the side boundary R is illustrated in Fig. 3 for the same slab geometry and properties, and for a target located in the midplane of the slab at the distance $x_s = x_1 + R$ from the side boundary. These figures support the general assumption that the influence of a lateral boundary on time-resolved measurements only becomes highly significant when the distance between the source-detector axis and the boundary is less than about half the total thickness of the slab.

III. MODEL VALIDATION

A. Monte Carlo model

In principle, Monte Carlo (MC) methods are able to simulate photon migration for any set of physical circumstances, and consequently have been employed as a means of validating other modeling schemes which generally involve simplifying assumptions. The trajectories of individual photons are simulated according to statistical rules which govern photon interactions within the medium. The research team at the University of Florence has, over a period of many years, developed a sophisticated MC model based on scaling relationships.[11] Although the computer code makes use of Mie scattering functions, to significantly reduce computation time and the disk memory requirements, the results reported here have been obtained by assuming an asymmetry factor g equal to zero, corresponding to Raleigh scatterers. Compared to the appropriately scaled results for nonzero g values, this approach produces only a very slight discrepancy near the source or for photons with very short flight times. The Florence model has been used extensively to study photon migration through slab geometries. The ability to simulate a diverse set of physical properties has been achieved by pre-

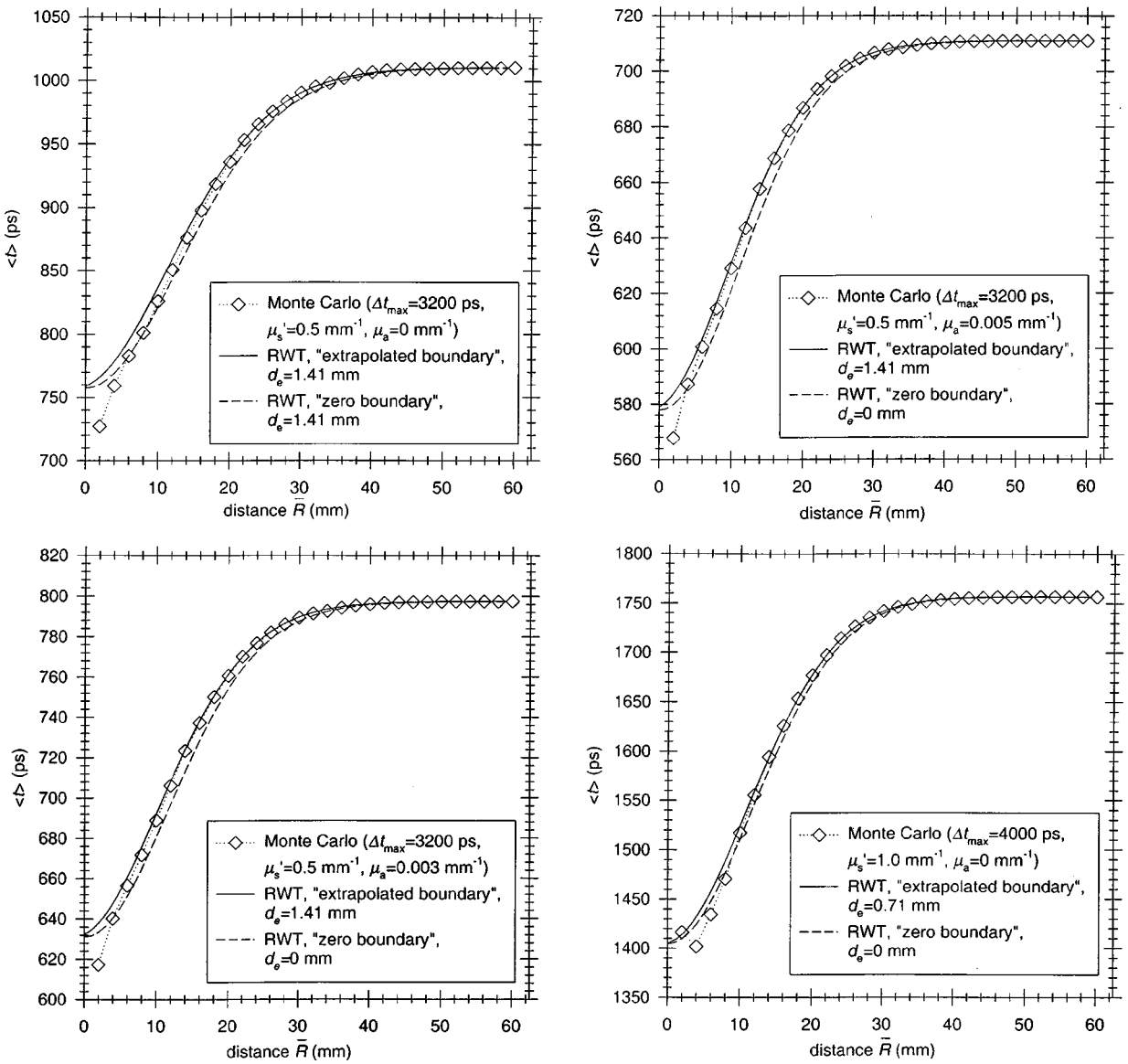

FIG. 5. (a)–(f) Curves of the mean flight time near the side boundary for $\mu_s'=0.5$, and 1.0 mm^{-1}, $\mu_a=0.0$, 0.003, and 0.005 mm^{-1}, respectively (comparison of the RWM estimates with the results of the Monte Carlo simulations. (g) Dependence of the mean flight time near the side boundary on the t_{max} of the Monte Carlo simulations for $\mu_s'=1.0$ mm^{-1}, $\mu_a=0.0$ mm^{-1}).

computing the trajectories of many thousands of transmitted photons for homogenous media with zero absorption and a refractive index of unity. Thereafter, the stored trajectories are appropriately weighted according to the distribution of absorption within the slab, making use of scaling relationships. Appropriate weights can also be used to simulate the behavior of scattering inhomogeneities.[11]

The University of Florence MC model was employed to derive the temporal distribution of photons transmitted between a source and detector aligned on opposite sides of a slab of thickness $T=40$ mm. The optical properties were $\mu_s'=0.5$ or 1.0 mm^{-1}, and $\mu_a=0.$, 0.003, or 0.005 mm^{-1}. A total of 30,000 trajectories were recorded using a detector which accepts photons over all angles of incidence within a radius of 2 mm. These data were then used to estimate the intensity and mean photon flight time as a function of the distance $\bar{R}$ between the source-detector axis and a totally absorbing side boundary. In practice, intensity and mean time estimates were calculated using all trajectories with flight times less than 3200 or 4000 ps for $\mu_s'=0.5$ or 1.0 mm^{-1}, respectively. Figures 4 and 5 show a comparison between the MC model results and the predictions of the RWT model as expressed by Eqs. (6) and (7), respectively. Each figure consists of six sets of curves corresponding to the three values of the absorption coefficient. The intensity curves in Figs. 4(a)–4(f) are shown on a logarithmic scale, and represent the results of the RWT calculations for the ''zero'' and ''extrapolated boundary'' conditions ($z_e=0.71/\mu_s'$ for the considered refraction index of the slab $n_r=1$). The MC model intensities were calculated by dividing the number of detected photons by the number of photons

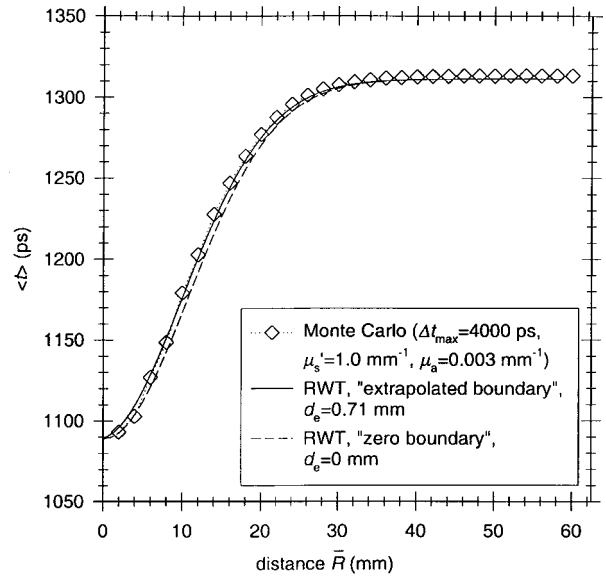

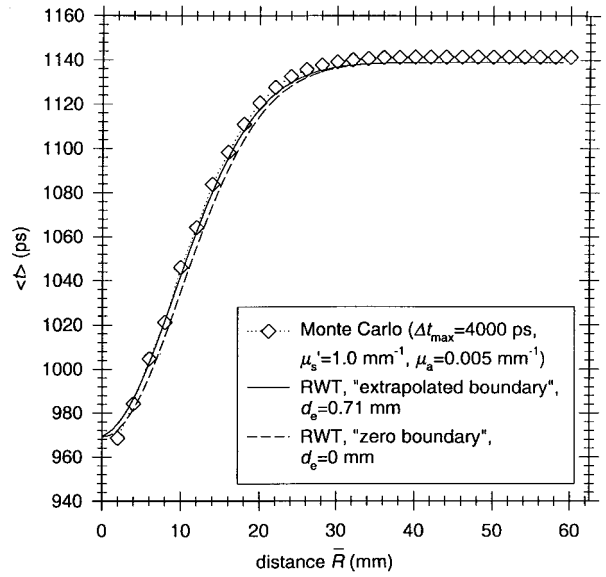

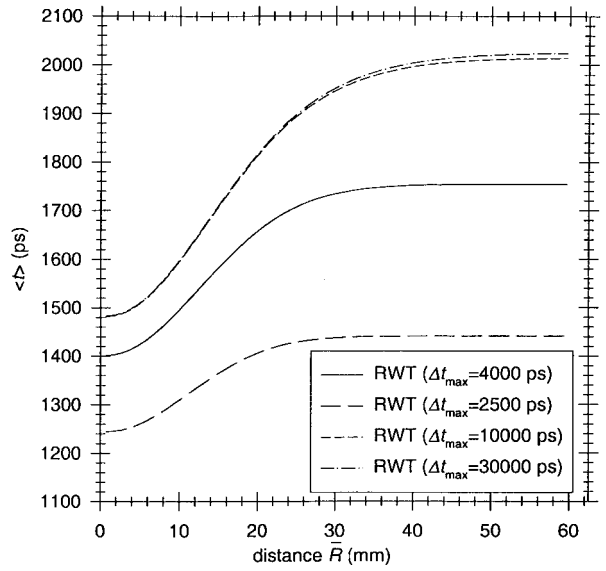

FIG. 5. (*Continued.*)

launched into the medium, and then dividing by the area of the detector.

In accordance with the scaling relationships Eq. (3), to compare the intensity found from MC (in $\mathrm{mm}^{-2}\,\mathrm{ps}^{-1}$) and corresponding probability estimated from RWT, we should multiply the latter by the dimensional factor $K=(c/\mu_s')\times(\sqrt{2}/\mu_s')^2=2c(\mu_s')^3$ (in fact, we take into account both the effective area S of the RWT ''detector,'' which is equal to the area of the lattice unit $S=(\sqrt{2}/\mu_s')^2$ and the relation between the step of the photon random walk and time $\delta t=(c\mu_s')^{-1}$).

Figures 4(a)–4(f) demonstrate that a very good agreement is obtained between the RWT curve for the ''extrapolated boundary'' condition and the Monte Carlo results. Accuracy of the RWT model proved to be better than 3%. The ''zero boundary'' condition gives qualitatively correct but less accurate results (especially, as can be expected, for smaller values μ_s' which correspond to larger z_e).

The RWT results in Figs. 5(a)–5(f) show the predicted variation in mean flight time $\langle t\rangle$ as the source-detector axis approaches the side boundary for a similar range of flight-time maxima. It is compared with the MC model. In all cases, accuracy of the RWT for the ''extrapolated boundary'' condition is again not worse than 3%.

It is worth noting that RWT formulas can be used to calculate in advance the maximum measured flight time sufficient to provide an accurate estimate of the mean. For example, in the case of $\mu_s'=0$, the $\Delta t_{\max}$ of 4000 ps selected for the Monte Carlo model in the case of $\mu_s'=1.0\,\mathrm{mm}^{-1}$ proved to be insufficient, and a value of $\Delta t_{\max}$ of 10 000 ps would have been more appropriate. The dependence of estimated $\langle t\rangle$ values on the $\Delta t_{\max}$ is illustrated by Fig. 5(g).

B. Experimental results

To explore the validity of the RWT model further, an experimental study was performed of the influence of lateral boundaries on time-resolved transmitted imensity measurements across a homogenous tissue-like slab. The experiments were performed at University College London using a system based on a Ti:sapphire laser and a streak camera. A solid homogenous slab was cast from a suspension of titanium dioxide particles and a NIR dye in epoxy resin, according to a recipe developed by Firbank and Delpy.[28] The predicted optical properties of the slab at a wavelength of 800 nm were $\mu_s'=1.0\,\mathrm{mm}^{-1}$ and $\mu_a=0.01\,\mathrm{mm}^{-1}$, and a refractive index of 1.56. The thickness of the slab was 35 mm, and the lengths along the other two dimensions were both 106 mm. Pulses from the laser were delivered to the surface of the slab via an optical fiber, with a mean power of about 400 mW at a wavelength of 800 nm. The transmitted signal was then relayed to the streak camera via a fiber bundle aligned precisely with the source fiber across the 35 mm thickness of the slab. The source-detector axis was initially aligned along the center of one side, 53 mm from the top and bottom surfaces of the slab. The temporal distribution of transmitted light, known as the temporal point spread function (TPSF), was then acquired by recording the transmitted signal over a

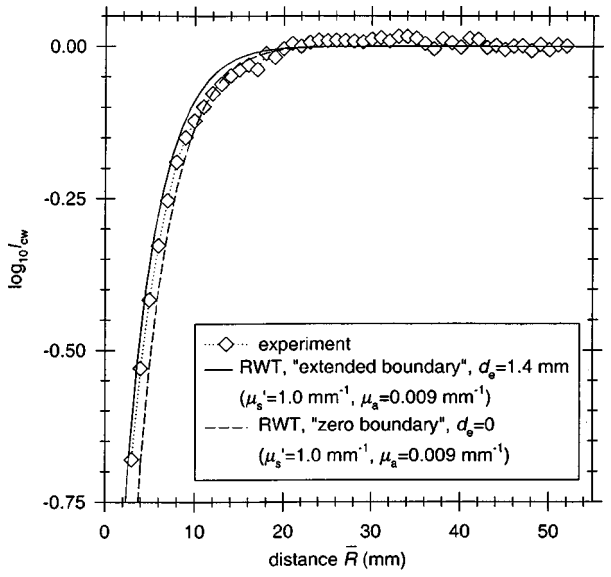

FIG. 6. Curves of the cw intensity near the side boundary (comparison of the RWM with the experimental data).

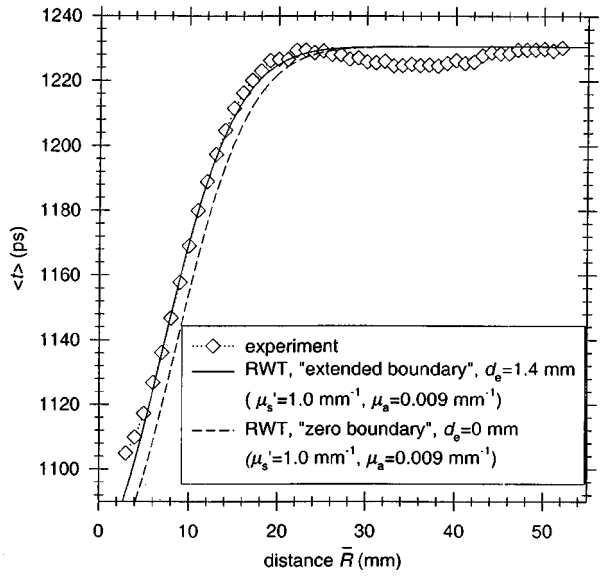

FIG. 7. Curves of the mean flight time near the side boundary (comparison of the RWM with the experimental data).

5 s period. The axis was then translated in 1 mm steps towards the center of the slab, in a direction parallel to the top and bottom surfaces. Data were recorded for a total translation of 50 mm. The instrumentation and the data acquisition process are described in greater detail elsewhere.[29,30] Following a routine series of calibrations,[30] the recorded TPSFs were used to calculate the relative intensity and mean flight time of the transmitted light. To confirm the optical properties of the slab, the TPSFs recorded at points furthest from the boundary were compared with a RWT model of the time-resolved transmittance,[17] which yielded values of $\mu_s' = 1.0\,\mathrm{mm}^{-1}$ and $\mu_a = 0.009\,\mathrm{mm}^{-1}$.

To substantially reduce the influence of the finite temporal window of the streak camera, least-squares fits of a diffusion-based analytical model were made to each recorded TPSF, which were then used to estimate intensity and mean flight time.[21] Although the model for a homogeneous slab medium did not account for the presence of lateral boundaries, by including arbitrary amplitude and temporal offset terms in the fitting process, very good quality fits were achieved.[21,29] Because streak cameras are not suitable for measuring absolute intensities, the data have been normalized to unity at the point furthest from the boundary.

Figure 6 shows the estimates of intensity compared to the predictions of the RWT model with negative image source (the lateral boundary is not perfectly reflecting). In fact, in the experimental setup the surface reflectance of this boundary has been further reduced by a black absorbing cover. Figure 7 shows the experimental estimates of mean flight time compared with the RWT model. Both assumptions concerning boundary conditions at the lateral surface of the slab (''zero boundary'' and ''extrapolated boundary'') were considered. Although agreement between the data and the RWT model with ''zero boundary'' condition is qualitatively good, the fit become better for the ''extrapolated boundary'' with $z_e = (\sqrt{2}/\mu_s') \approx 1.4\,\mathrm{mm}$. This value of z_e (equal to an additional lattice unit) is almost two times smaller than the estimated value found directly from the refraction index mismatch between the stab and the air[22,23] $z_e = (2.71/\mu_s')$, indicating the reduction in effective reflectivity of the lateral boundary from expected $R_{\mathrm{eff}} \approx 0.6$ to $R_{\mathrm{eff}} \approx 0.33$ due, possibly, to the decreased index mismatch between the phantom surface and its black cover.

IV. SUMMARY AND DISCUSSION

When a measurement is made of the optical signal transmitted between two points on the surface of a highly scattering medium such as tissue, it is dependent on more than simply the optical properties along the line of sight. The geometry and properties of the surrounding volume will influence all but the photons with the shortest possible flight-times. Geometrical effects have been shown to be a significant problem in the generation and interpretation of transillumination images. Recently, Fantini *et al.*[31] have explored a method to correct for the proximity of lateral boundaries in frequency-resolved transmittance measurements of the breast. A high degree of correction to AC modulation measurements was achieved using *a posteriori* information derived from the simultaneous measurement of phase delay.

Fast and efficient solution of the inverse problem in optical tomography would benefit from the application of a forward model that is expressible analytically. In this respect RWT is a powerful and versatile technique. RWT models have been developed for increasingly sophisticated geometries and internal distributions of optical properties. A method has been demonstrated here of modifying a random walk model to take account of the influence of lateral boundaries on the time-resolved signal through a uniform slab. The predictions of the model have been shown to be in very good agreement with those of a Monte Carlo model, and with

experimental results. The general method can easily be extended to handle additional lateral boundaries, although the resulting analytical expressions are necessarily complex. However, ultimate extension to arbitrary media may require the use of finite-element or finite-difference schemes.[6] In the near future, we expect to apply the modified time-resolved contrast functions described here to imaging and quantitative analysis of targets that are adjacent to lateral boundaries.

[1]D. T. Delpy and M. Cope, ''Quantification in tissue near-infrared spectroscopy,'' Philos. Trans. R. Soc. London, Ser. B **352**, 649–659 (1997).

[2]Proceedings of SPIE, *Optical Tomography and Spectroscopy of Tissue: Theory, Instrumentation, Model, and Human Studies II*, edited by B. Chance and R. R. Alfano, 1997, Vol. 2979.

[3]*Trends in Optics and Photonics on Advances in Optical Imaging and Photon Migration*, edited by R. R. Alfano and J. G. Fujimoto (OSA: Washington DC, 1996), Vol. 2.

[4]E. B. de Haller, ''Time-resolved transillumination and optical tomography,'' J. Biomed. Opt. **1**, 7–17 (1996).

[5]J. C. Hebden, S. R. Arridge, and D. T. Delpy, ''Optical imaging in medicine I: experimental techniques,'' Phys. Med. Biol. **42**, 825–840 (1997).

[6]S. R. Arridge and J. C. Hebden, ''Optical imaging in medicine II: modelling and reconstruction,'' Phys. Med. Biol. **42**, 841–854 (1997).

[7]B. Monsees, J. Destouet, and D. Gersell, ''Light scan evaluation of nonpalpable breast lesions,'' Radiology **163**, 467–470 (1987).

[8]B. Chance, M. Cope, E. Gratton, N. Ramanujam, and B. Tromberg, ''Phase measurement of light absorption and scatter in human tissue,'' Rev. Sci. Instrum. **69**, 3457–3481 (1998).

[9]B. C. Wilson and G. Adam, ''A Monte Carlo model for the absorption and flux distribution of light in tissue,'' Med. Phys. **10**, 824–830 (1983).

[10]L. H. Wang, S. L. Jacques, and L. Zheng, ''MCML-Monte Carlo modeling of light transport in multilayered tissues,'' Comput. Methods Programs Biomed. **47**, 131–146 (1995).

[11]A. Sassaroli, C. Blumetti, F. Martelli, D. Contini, A. Ismaelli, and G. Zaccanti, ''A Monte Carlo procedure for investigating light propagation and imaging of highly scattering media,'' Appl. Opt. **37**, 7392–7400 (1998).

[12]N. J. McCormick, ''A review of neutron transport approximations,'' Nucl. Sci. Eng. **80**, 481–535 (1982).

[13]A. H. Hielscher, R. F. Acouffe, and R. L. Barbour, ''Comparison of finite-difference transport and diffusion calculations for photon migration in homogeneous and inhomogeneous tissues,'' Phys. Med. Biol. **43**, 1285–1302 (1998).

[14]J.-M. Kaltenbach and M. Kaschke, ''Frequency and time domain modelling of light transport in random media,'' in *Medical Optical Tomography: Functional Imaging and Monitoring*, edited by G. J. Müller *et al.* (SPIE, Bellingham, WA, 1993), pp 65–86.

[15]R. F. Bonner, R. Nossal, S. Havlin, and G. H. Weiss, ''Model for photon migration in turbid biological media,'' J. Opt. Soc. Am. A **4**, 423–432 (1987).

[16]A. H. Gandjbakhche and G. H. Weiss, ''Random walk and diffusion-like models of photon migration in turbid media,'' in *Progress in Optics*, edited by E. Wolf (North–Holland, Amsterdam, 1995), Vol. 34, pp. 333–401.

[17]A. H. Gandjbakhche, G. H. Weiss, R. F. Bonner, and R. Nossal, ''Photon pathlength distributions for transmission through optically turbid slabs,'' Phys. Rev. E **48**, 810–818 (1993).

[18]V. Chernomordik, R. Nossal, and A. H. Gandjbakhche, ''Point spread functions of photons in time-resolved transillumination experiments using simple scaling argument,'' Med. Phys. **23**, 1857–1861 (1996).

[19]A. H. Gandjbakhche, R. F. Bonner, R. Nossal, and G. H. Weiss, ''Absorbtivity contrast in transillumination imaging of tissue abnormalities,'' Appl. Opt. **35**, 1767–1774 (1996).

[20]A. H. Gandjbakhche, V. Chernomordik, J. C. Hebden, and R. Nossal, ''Time-dependent contrast functions for quantitative imaging in time-resolved transillumination experiments,'' Appl. Opt. **37**, 1973–1981 (1998).

[21]M. Patterson, B. Chance, and B. C. Wilson, ''Time resolved reflectance and transmittance for the non-invasive measurement of tissue optical properties,'' Appl. Opt. **28**, 2331–2336 (1989).

[22]R. S. Haskell, L. O. Swaasand, T. T. Tsay, T. C. Feng, M. S. McAdams, and B. Tromberg, ''Boundary conditions for the diffusion equation in radiative transfer,'' J. Opt. Soc. Am. A **11**, 2727–2741 (1994).

[23]R. Aronson, ''Boundary conditions for diffusion of light,'' J. Opt. Soc. Am. A **12**, 2532–2539 (1995).

[24]M. U. Vera and D. J. Durian, ''Angular distribution of diffusively transmitted light,'' Phys. Rev. E **53**, 3215–3224 (1996).

[25]D. Contini, F. Martelli, and G. Zaccanti, ''Photon migration through a turbid slab described by a model based on diffusion approximation I. Theory,'' Appl. Opt. **36**, 4587–4599 (1997).

[26]M. Keijzer, W. M. Star, and P. R. M. Storchi, ''Optical diffusion in layered media,'' Appl. Opt. **27**, 1820–1824 (1988).

[27]A. H. Hielscher, S. L. Jacques, L. Wang, and F. K. Tittel, ''The influence of boundary conditions on the accuracy of diffusion theory in time-resolved reflectance spectroscopy of biological tissues,'' Phys. Med. Biol. **40**, 1957–1975 (1995).

[28]M. Firbank and D. T. Delpy, ''A design for a stable and reproducible phantom for use in near-infrared imaging and spectroscopy,'' Phys. Med. Biol. **38**, 847–853 (1993).

[29]J. C. Hebden and D. T. Delpy, ''Enhanced time-resolved imaging with a diffusion model of photon transport,'' Opt. Lett. **19**, 311–313 (1994).

[30]J. C. Hebden, D. J. Hall, and D. T. Delpy, ''The spatial resolution performance of a time-resolved optical imaging system using temporal extrapolation,'' Med. Phys. **22**, 201–208 (1995).

[31]S. Fantini, M. A. Franceschini, G. Gaida, E. Gratton, H. Jess, W. W. Mantulin, K. T. Moesta, P. M. Schlag, and M. Kaschke, ''Frequency-domain optical mammography: edge effect corrections,'' Med. Phys. **23**, 149–157 (1996).